Universität Potsdam

Fred Feudel, Norbert Seehafer

On the bifurcation phenomena in truncations of the 2D Navier-Stokes

NLD Preprints ; 1

On the Bifurcation Phenomena in Truncations of the 2D Navier-Stokes Equations

FRED FEUDEL and NORBERT SEEHAFER
Max-Planck-Gruppe Nichtlineare Dynamik, Universität Potsdam,
PF 601553, D-14415 Potsdam, Germany

Abstract

We have studied bifurcation phenomena for the incompressible Navier-Stokes equations in two space dimensions with periodic boundary conditions. Fourier representations of velocity and pressure have been used to transform the original partial differential equations into systems of ordinary differential equations (ODE), to which then numerical methods for the qualitative analysis of systems of ODE have been applied, supplemented by the simulative calculation of solutions for selected initial conditions. Invariant sets, notably steady states, have been traced for varying Reynolds number or strength of the imposed forcing, respectively. A complete bifurcation sequence leading to chaos is described in detail, including the calculation of the Lyapunov exponents that characterize the resulting chaotic branch in the bifurcation diagram.

1 INTRODUCTION

The study of truncations of the fluid dynamic equations began with the seminal paper of Lorenz [1], who studied a three-mode model for Rayleigh-Bénard convection.

In 1979 Franceschini and his co-workers started a systematic investigation of the qualitative behaviour of solutions to truncations of the 2D incompressible Navier-Stokes equations (NSE) with periodic boundary conditions [2, 3, 4, 5]. They applied a special, constant and real, forcing at one selected Fourier mode and analyzed the bifurcations occuring when the strength of the forcing is varied. Beginning with a rather strong truncation, namely a five-mode model, they included more and more modes in their study (up to 1000). In particular, they investigated the influence of the number of modes on the bifurcation structure, with the aim to estimate the minimal number of modes to be retained in a truncation model. More recently Franceschini and Zanasi [6] turned to the study of the 3D NSE, applying the same forcing as in the 2D case, but hitherto only for a seven-mode truncation.

Jolly [7] used the concept of approximate inertial manifolds (AIMs) to study the bifurcation structure of the 2D NSE. He found that the AIM concept, also referred to as nonlinear Galerkin method, reduces the number of modes needed to capture certain bifurcations compared with the traditional Galerkin method.

The up to now most detailed bifurcation study of the 2D NSE is due to Lee [8], who used a forcing different from that applied by Franceschini and his co-workers. The changes in the solution behaviour which he observed for varying Reynolds number or strength of the forcing, respectively, are extremely complex. It is the aim of the present paper to continue Lee's study and to describe the bifurcation behaviour on a systematic base.

In Section 2 we transform the 2D NSE into spectral form. Analytic expressions for the Jacobian matrix of the resulting system of ordinary differential equations (ODE), useful for the application of numerical methods of bifurcation analysis, such as path following in the bifurcation diagram, are given in the Appendix.

Then in Sections 3 and 4 the complete bifurcation sequence leading to chaos is presented. The appearance of a chaotic state is verified by calculating the Lyapunov exponents.

Section 5, finally, contains a brief discussion of our results.

2 BASIC EQUATIONS AND TRUNCATION MODEL

We start from the non-dimensional equations for an incompressible fluid with constant material properties,

$$\frac{\partial \mathbf{v}}{\partial t} + (\mathbf{v} \cdot \operatorname{grad})\mathbf{v} = R^{-1} \triangle \mathbf{v} - \operatorname{grad} p + \mathbf{f}, \tag{1}$$

$$\operatorname{div} \mathbf{v} = 0, \tag{2}$$

where $\mathbf{v}$ and p denote the dimensionless fluid velocity and thermal pressure, R the Reynolds numbers, and $\mathbf{f}$ a yet unspecified body force.

We restrict ourselves to the 2D case and apply periodic boundary conditions on a square region of side length 2π, which is equivalent to considering the motion on the torus $T^2 = [0, 2\pi] \times [0, 2\pi]$. The mean values of $\mathbf{v}$ and consequently also of $\mathbf{f}$ are assumed to vanish,

$$\int_{T^2} \mathbf{v} \, \mathrm{d}^2\mathbf{x} = \mathbf{0}, \quad \int_{T^2} \mathbf{f} \, \mathrm{d}^2\mathbf{x} = \mathbf{0}. \tag{3}$$

The periodicity assumption implies that the Fourier representations of $\mathbf{v}$, p and $\mathbf{f}$,

$$\mathbf{v}(\mathbf{x}) = \sum_{\substack{\mathbf{k} \in \mathbb{Z}^2 \\ \mathbf{k} \neq \mathbf{0}}} \mathbf{v}_\mathbf{k} \exp(\mathrm{i}\mathbf{k} \cdot \mathbf{x}), \tag{4}$$

$$p(\mathbf{x}) = \sum_{\mathbf{k} \in \mathbb{Z}^2} p_\mathbf{k} \exp(\mathrm{i}\mathbf{k} \cdot \mathbf{x}), \quad \mathbf{f}(\mathbf{x}) = \sum_{\substack{\mathbf{k} \in \mathbb{Z}^2 \\ \mathbf{k} \neq \mathbf{0}}} \mathbf{f}_\mathbf{k} \exp(\mathrm{i}\mathbf{k} \cdot \mathbf{x}), \tag{5}$$

can be differentiated term by term with respect to the spatial coordinates. In the Fourier space the incompressibility condition, equation (2), takes the form

$$\mathbf{v}_\mathbf{k} \cdot \mathbf{k} = 0 \tag{6}$$

and is automatically satisfied if we write

$$\mathbf{v_k} = v_\mathbf{k}\mathbf{e_k} \qquad \text{for } \mathbf{k} \neq \mathbf{0}, \tag{7}$$

with (real) "polarization" vectors $\mathbf{e_k}$ perpendicular to $\mathbf{k}$,

$$\mathbf{e_k} \cdot \mathbf{k} = 0, \quad \mathbf{e_k}^2 = 1, \quad \mathbf{e_{-k}} = \mathbf{e_k}. \tag{8}$$

The last condition in equation (8) ensures that

$$v_{-\mathbf{k}} = v_\mathbf{k}^* \tag{9}$$

for real $\mathbf{v}(\mathbf{x})$. By using this representation for $\mathbf{v_k}$ we furthermore easily get rid of the pressure term in equation (1) and arrive at the following infinite-dimensional system of ODE:

$$\frac{\mathrm{d}v_\mathbf{k}}{\mathrm{d}t} = -R^{-1}\mathbf{k}^2 v_\mathbf{k} - \mathrm{i} \sum_{\substack{\mathbf{p},\mathbf{q}\in\mathbb{Z}^2 \\ \mathbf{p},\mathbf{q}\neq\mathbf{0};\, \mathbf{p}+\mathbf{q}=\mathbf{k}}} (\mathbf{e_p}\cdot\mathbf{k})(\mathbf{e_q}\cdot\mathbf{e_k}) v_\mathbf{p} v_\mathbf{q} + f_\mathbf{k}. \tag{10}$$

$f_\mathbf{k}$ on the right of equation (10) is defined by

$$f_\mathbf{k} = \mathbf{f_k} \cdot \mathbf{e_k}. \tag{11}$$

For our numerical calculations on a vectorizing computer (CRAY YMP–EL) it has been advantageous to replace the double sum in equation (10) by a simple sum by means of the substitution $\mathbf{q} = \mathbf{k} - \mathbf{p}$, so that

$$\frac{\mathrm{d}v_\mathbf{k}}{\mathrm{d}t} = -R^{-1}\mathbf{k}^2 v_\mathbf{k} - \mathrm{i} \sum_{\substack{\mathbf{p}\in\mathbb{Z}^2 \\ \mathbf{p}\neq\mathbf{0},\mathbf{k}}} (\mathbf{e_p}\cdot\mathbf{k})(\mathbf{e_{k-p}}\cdot\mathbf{e_k}) v_\mathbf{p} v_\mathbf{k-p} + f_\mathbf{k}. \tag{12}$$

Because of the reality condition (9), we can restrict ourselves to $\mathbf{k}$ vectors in a subset $\mathbb{K}^2$ of $\mathbb{Z}^2$ defined by

$$\mathbb{K}^2 \stackrel{\text{def}}{=} \{\mathbf{k} \in \mathbb{Z}^2 : k_1 > 0\} \cup \{\mathbf{k} \in \mathbb{Z}^2 : k_1 = 0 \wedge k_2 > 0\}. \tag{13}$$

In the following we shall use the additional definitions

$$\langle\mathbf{k}\rangle \stackrel{\text{def}}{=} \begin{cases} \mathbf{k} : \mathbf{k} \in \mathbb{K}^2 \\ -\mathbf{k} : \mathbf{k} \notin \mathbb{K}^2 \end{cases} \tag{14}$$

and

$$\mathrm{sgn}(\mathbf{k}) \stackrel{\text{def}}{=} \frac{\mathbf{k}\cdot\langle\mathbf{k}\rangle}{\mathbf{k}^2}. \tag{15}$$

From equation (12) we then obtain our final equations for the time evolution of the real and imaginary parts of $v_\mathbf{k}$ in the forms

$$\begin{aligned} \frac{\mathrm{d}v_\mathbf{k}^{\mathrm{Re}}}{\mathrm{d}t} \;=\; & -R^{-1}\mathbf{k}^2 v_\mathbf{k}^{\mathrm{Re}} + \sum_{\substack{\mathbf{p}\in\mathbb{K}^2 \\ \mathbf{p}\neq\mathbf{k}}} (\mathbf{e_p}\cdot\mathbf{k}) \Big\{ (\mathbf{e}_{\langle\mathbf{k-p}\rangle}\cdot\mathbf{e_k}) \Big[\mathrm{sgn}(\mathbf{k}-\mathbf{p}) v_\mathbf{p}^{\mathrm{Re}} v_{\langle\mathbf{k-p}\rangle}^{\mathrm{Im}} \\ & + v_\mathbf{p}^{\mathrm{Im}} v_{\langle\mathbf{k-p}\rangle}^{\mathrm{Re}} \Big] \\ & + (\mathbf{e_{k+p}}\cdot\mathbf{e_k}) \Big[v_\mathbf{p}^{\mathrm{Re}} v_\mathbf{k+p}^{\mathrm{Im}} - v_\mathbf{p}^{\mathrm{Im}} v_\mathbf{k+p}^{\mathrm{Re}} \Big] \Big\} \\ & + f_\mathbf{k}^{\mathrm{Re}}, \end{aligned} \tag{16}$$

$$\begin{aligned}\frac{\mathrm{d}v_{\mathbf{k}}^{\mathrm{Im}}}{\mathrm{d}t} &= -R^{-1}\mathbf{k}^2 v_{\mathbf{k}}^{\mathrm{Im}} - \sum_{\substack{\mathbf{p}\in\mathbb{K}^2\\ \mathbf{p}\neq\mathbf{k}}} (\mathbf{e}_{\mathbf{p}}\cdot\mathbf{k})\Big\{(\mathbf{e}_{\langle\mathbf{k}-\mathbf{p}\rangle}\cdot\mathbf{e}_{\mathbf{k}})\Big[v_{\mathbf{p}}^{\mathrm{Re}} v_{\langle\mathbf{k}-\mathbf{p}\rangle}^{\mathrm{Re}} \\ &\quad - \mathrm{sgn}(\mathbf{k}-\mathbf{p}) v_{\mathbf{p}}^{\mathrm{Im}} v_{\langle\mathbf{k}-\mathbf{p}\rangle}^{\mathrm{Im}}\Big] \\ &\quad + (\mathbf{e}_{\mathbf{k}+\mathbf{p}}\cdot\mathbf{e}_{\mathbf{k}})\Big[v_{\mathbf{p}}^{\mathrm{Re}} v_{\mathbf{k}+\mathbf{p}}^{\mathrm{Re}} + v_{\mathbf{p}}^{\mathrm{Im}} v_{\mathbf{k}+\mathbf{p}}^{\mathrm{Im}}\Big]\Big\} \\ &\quad + f_{\mathbf{k}}^{\mathrm{Im}}. \end{aligned} \tag{17}$$

We have used an isotropic truncation in wave number space, following Lee [9, 8], who segmented the $\mathbf{k}$ space into successive rings $n^2 - n < \mathbf{k}^2 \leq n^2 + n$, $n = 1, 2, \cdots$. If not indicated differently, the rings up to $n = 8$ have taken into account in our numerical calculations, altogether 112 $\mathbf{k}$-vectors, which amounts to studying a system of 224 ODE.

Because of the periodic boundary conditions, the total energy flow through the boundary of the region considered vanishes, so that in order to compensate for viscous losses some kind of external forcing has to be applied. We have used a constant, single-mode forcing at $\mathbf{k} = (4, 1)$, with equal strength in the real and imaginary parts:

$$f_{\mathbf{k}} = \begin{cases} f + \mathrm{i}f : \mathbf{k} = (4,1) \\ 0 : \mathbf{k} \neq (4,1) \end{cases} \tag{18}$$

For this special type of forcing the NSE remains invariant with respect to translations perpendicular to the $\mathbf{k}$ vector of the forced mode. f on the right of equation (18) is our bifurcation parameter, while the Reynolds number R was kept fixed at a value of 50 throughout the calculations.

3 BIFURCATIONS OF STEADY STATES AND TRAVELLING WAVES

We now begin the description of the complex bifurcation sequence, which eventually leads to chaos. Fig. 1 gives an overview of the steady states and their bifurcations, showing the dependence of the modulus of the forced velocity mode (vertical axis) on the bifurcation parameter f. Thick lines indicate stable branches. The solution branches have been continued by means of a predictor-corrector method. In each step the eigenvalues of the Jacobian matrix were calculated to detect bifurcation points.

Unstable steady-state branches have been followed only in a certain neighbourhood of the stable branch. Each unstable branch showed a complex sequence of tertiary bifurcations (not drawn in Fig.1), in which the degree of instability, namely the number of eigenvalues of the Jacobian matrix with positive real parts, increased. None of the unstable branches was observed to return to the stable branch.

For very small values of f the forced mode is the only one present in the steady state. The streamlines of the resulting velocity field are straight lines perpendicular to the wave vector of the forced mode. This trivial steady state loses its stability

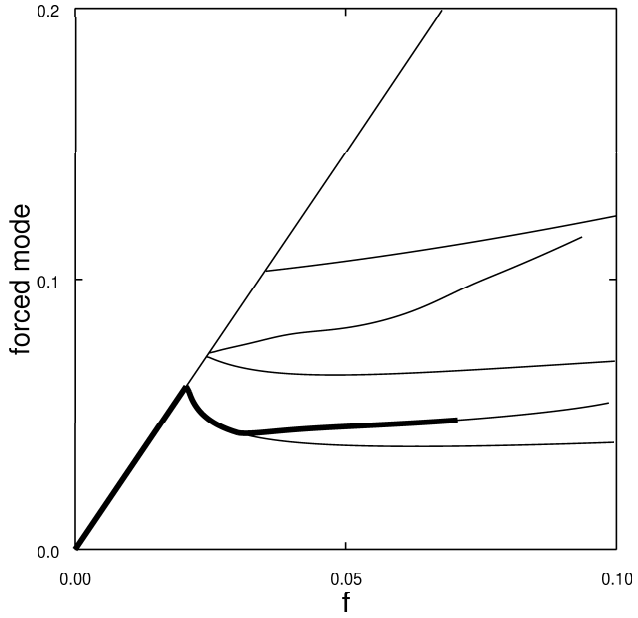

Figure 1: Bifurcation diagram for the steady states.

at $f = f_1 = 0.0206$, where two eigenvalues go through zero. The degeneracy results from the translational symmetry mentioned in Section 2 and the bifurcation breaks the symmetry of the original steady state. The new stable solutions are no longer symmetric and one eigenvalue of the Jacobian matrix is permanently equal to zero along the solution branch. Now more modes than one, but not yet all, are excited. The remaining modes become different from zero in the next bifurcation at $f = f_2 = 0.0301$.

The stable steady-state branch ends up in a special bifurcation at $f = f_3 = 0.0706$, leading to travelling waves (TW). At this bifurcation point a second eigenvalue, in addition to that already vanishing along the whole branch, becomes zero, whereby the eigenvectors belonging to these two eigenvalues align with one another. An analogous phenomenon has been observed by Kevrekidis *et al.* [10] for the Kuramoto-Sivashinsky equation. With the exception of the forced mode and the modes with wave vectors parallel to that of the forced mode, all modes describe circles in the planes spanned by their respective real and imaginary parts, with rational ratios between the rotation frequencies for different modes. The latter can be seen from Lissajous figures as shown in Fig. 2. The forced mode and the other non-rotating modes are constant in time. Rotating modes with parallel $\mathbf{k}$ vectors have equal ratios $\omega^2/\mathbf{k}^2$, ω denoting the rotation frequency, so that their superposition is even a solution of the linear wave equation. For the resulting TW the whole velocity field is moving with a constant speed in the direction of the translational invariance of the equations.

The TW solution loses stability in a bifurcation at $f = f_4 = 0.087$, where also the forced mode begins to oscillate, causing the transition to a modulated travelling

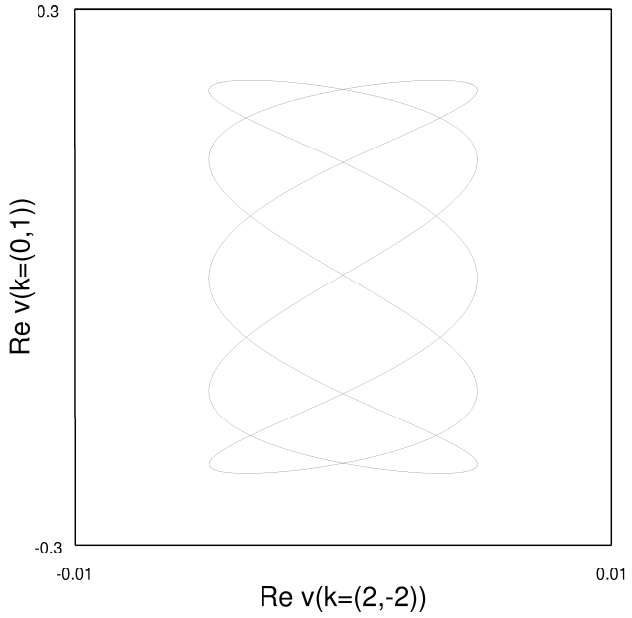

Figure 2: Lissajous figure produced by the projection of a trajectory onto the plane spanned by the real parts of two different modes for $f = 0.08$.

wave (MTW), which represents a first, nongeneric torus solution.

4 TORUS SOLUTIONS, PHASE LOCKINGS AND A TRANSITION TO CHAOS

The branch opened by the transition to the MTW at $f = f_4$ is shown schematically in Fig. 3. Now also the forced mode and the total energy in the velocity field, both constant up to this bifurcation, vary in time.

The following figures show, for different values of the forcing parameter f, system trajectories in projection on two selected planes, spanned by the real and imaginary parts of the $\mathbf{k} = (2, -2)$ mode and of the forced mode, respectively (cf. Lee [8]). In Fig. 4, where the $(2, -2)$-mode is drawn for a parameter value only slightly above f_4, two frequencies are plainly recognizable. The lower of them corresponds to the oscillation of the mode already present for the TW, caused by the wave propagation in connection with the periodic boundary conditions. The other is the oscillation frequency of the forced mode, which is purely periodic at this stage, at which also the moduli of the other modes are purely periodic with the same frequency. This property distinguishes an MTV from a generic torus.

At $f = f_5 = 0.092$ the forced mode becomes non-periodic. The appearance of a new frequency leads to the generation of a generic torus. A further increase of the forcing leads to a phase locking ($f = f_6 = 0.0929$) and a completely periodic orbit arises (Figs. 6 and 7).

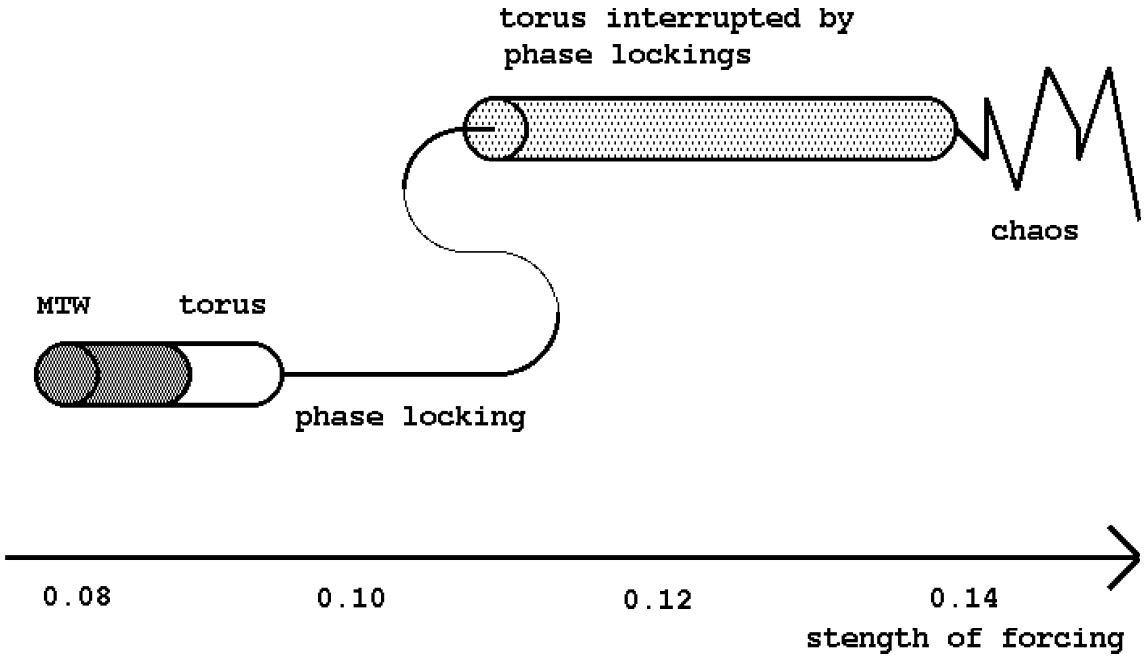

Figure 3: Schematic bifurcation diagram for the torus, phase locking and chaotic solutions.

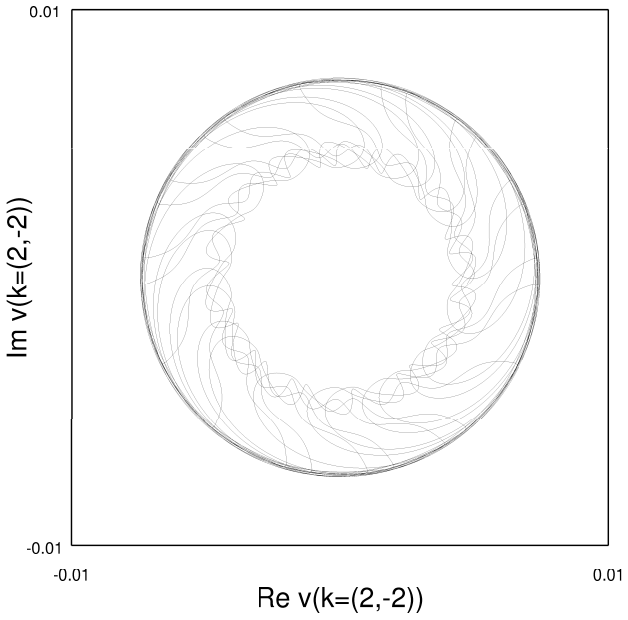

Figure 4: Projection of the torus solution for $f = 0.089$ onto the plane spanned by the real and imaginary parts of the $\mathbf{k} = (2, -2)$ mode.

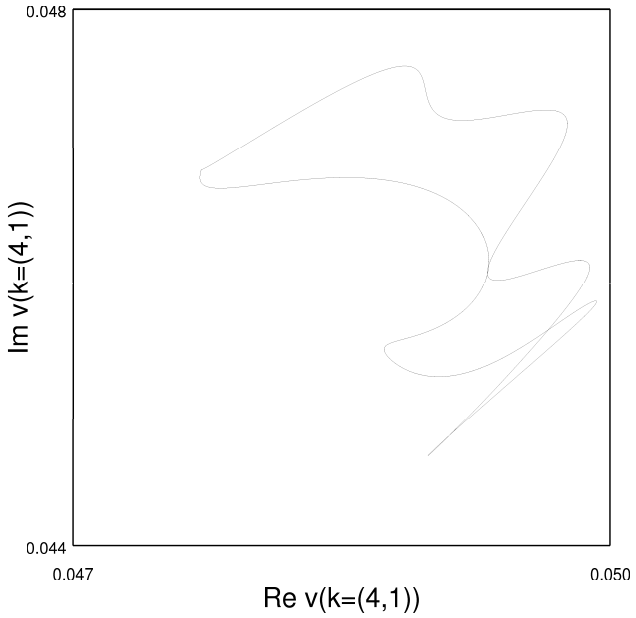

Figure 5: Projection of the torus solution for $f = 0.089$ onto the plane spanned by the real and imaginary parts of the forced mode ($\mathbf{k} = (4, 1)$).

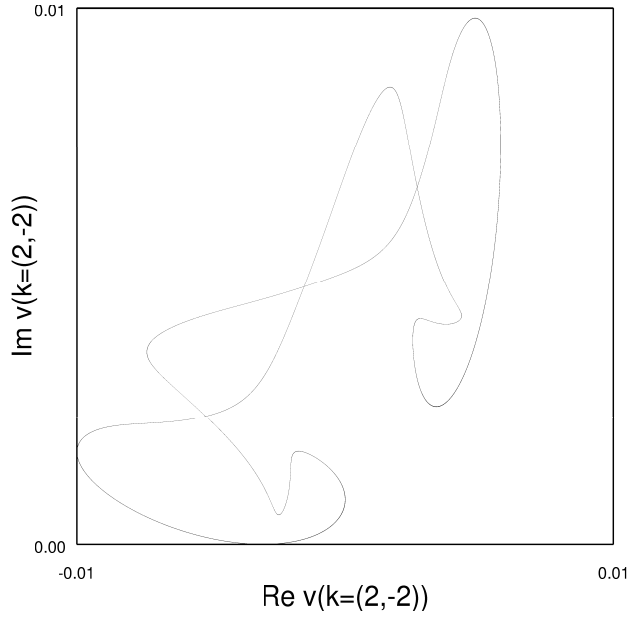

Figure 6: Projection of the phase-locking periodic solution for $f = 0.1072$ onto the plane spanned by the real and imaginary parts of the $\mathbf{k} = (2, -2)$ mode (lower branch in Fig. 3).

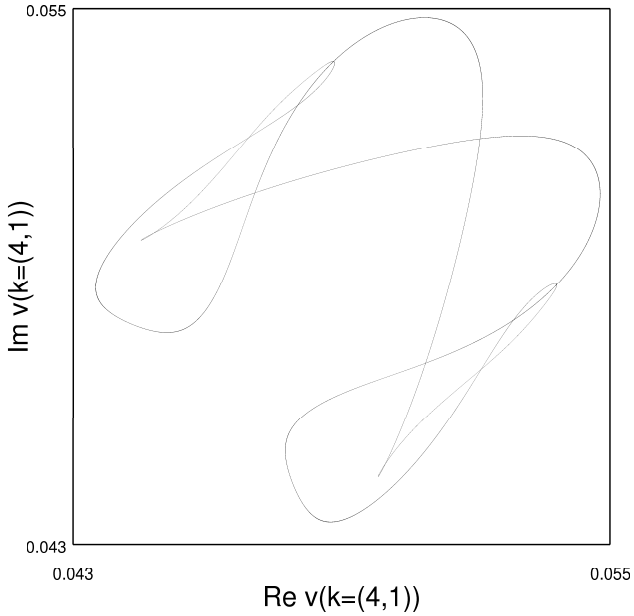

Figure 7: Projection of the phase-locking periodic solution for $f = 0.1072$ onto the plane spanned by the real and imaginary parts of the forced ($\mathbf{k} = (4, 1)$) mode (lower branch in Fig. 3).

This periodic solution was followed up to $f = f_7 = 0.1092$ and could then no longer be observed. But for $f = f_8 = 0.1071$ a new periodic orbit was detected (Figs. 8 and 9), coexisting with the former one. Because of the similarity of both solutions (cf. Figs. 6 and 7 with Figs. 8 and 9) we suppose a connection of both branches over two turning points with an unstable solution in between, as indicated in Fig. 3. A more detailed analysis of this parameter range is under way.

The new periodic orbit in turn bifurcates to a torus solution at $f = f_9 = 0.1080$. This torus branch exists for a larger interval of f, interrupted by several phase lockings. In Figs. 10 and 11 a trajectory belonging to this branch is drawn. It seems to show phase locking with a large frequency ratio. For other values of the bifurcation parameter the torus is completely filled.

With a further increase of the forcing parameter, finally, the torus disappears and chaos occurs. In Figs. 12 and 13 the chaotic trajectory is drawn for the parameter value $f = 0.14$, for which, in order to verify the chaotic character of the solution, the (10) largest Lyapunov exponents have been calculated. The largest of them is positive, the next two are equal to zero, and the following are negative. One of the vanishing exponents belongs to the direction of the trajectory, the other results from the continuous symmetry of the system.

The Lyapunov exponents can be used to calculate the Kaplan-Yorke dimension D_{KY} of the attractor, which is a good approximation of its Hausdorff dimension [11]. If the Lyapunov exponents λ_i are ordered descendingly and j is the largest index

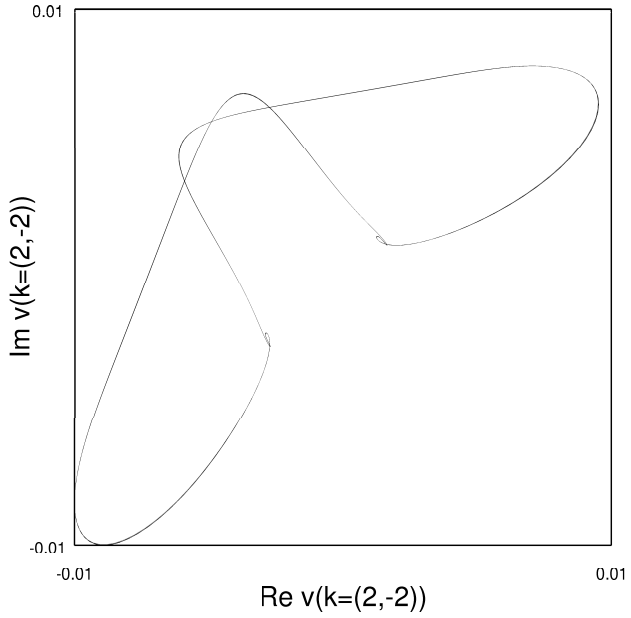

Figure 8: Projection of the coexisting periodic solution for $f = 0.1072$ onto the plane spanned by the real and imaginary parts of the $\mathbf{k} = (2, -2)$ mode (upper branch in Fig. 3).

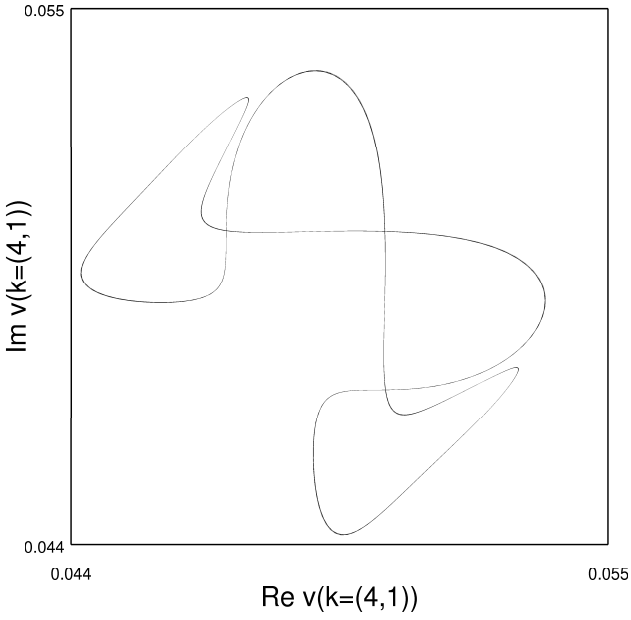

Figure 9: Projection of the coexisting periodic solution for $f = 0.1072$ onto the plane spanned by the real and imaginary parts of the forced ($\mathbf{k} = (4, 1)$) mode (upper branch in Fig. 3).

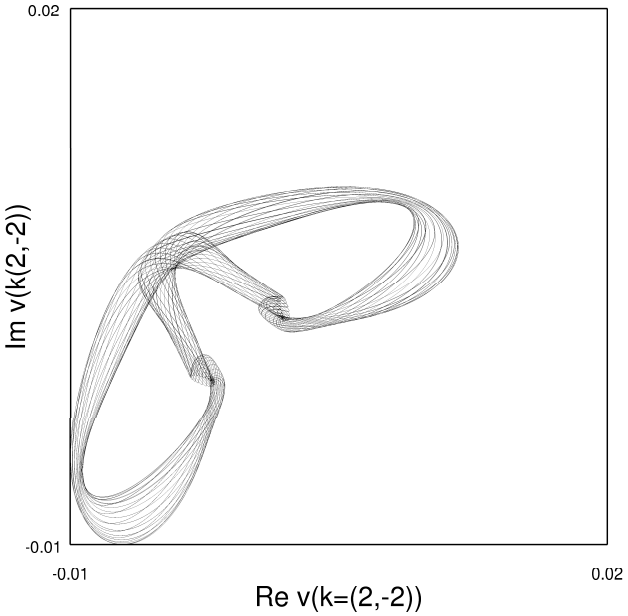

Figure 10: Projection of the phase-locking periodic solution for $f = 0.11$ onto the plane spanned by the real and imaginary parts of the $\mathbf{k} = (2, -2)$ mode (upper branch in Fig. 3).

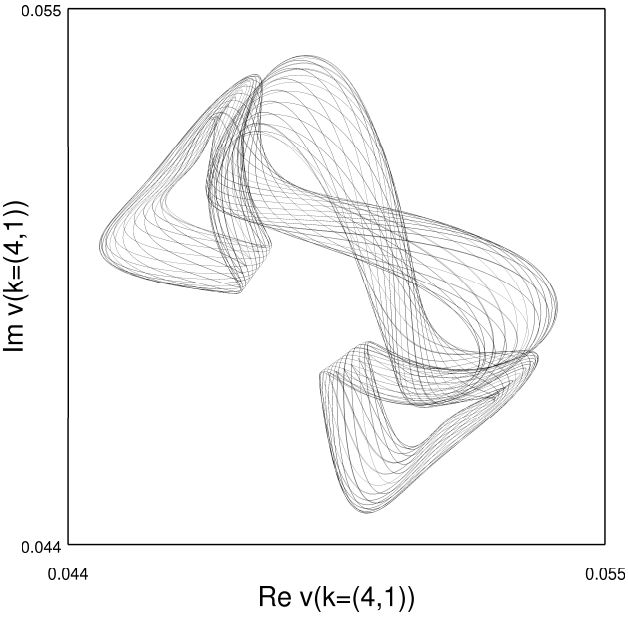

Figure 11: Projection of the phase-locking periodic solution for $f = 0.11$ onto the plane spanned by the real and imaginary parts of the forced ($\mathbf{k} = (4, 1)$) mode (upper branch in Fig. 3).

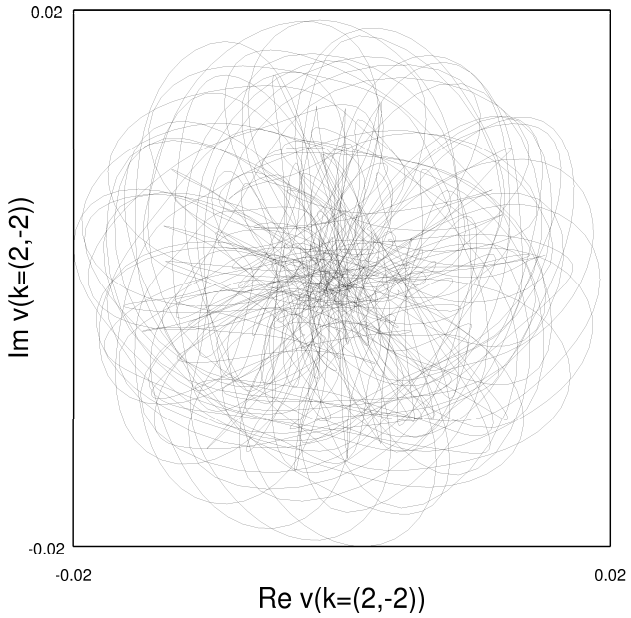

Figure 12: Projection of the chaotic solution for $f = 0.14$ onto the plane spanned by the real and imaginary parts of the $\mathbf{k} = (2, -2)$ mode.

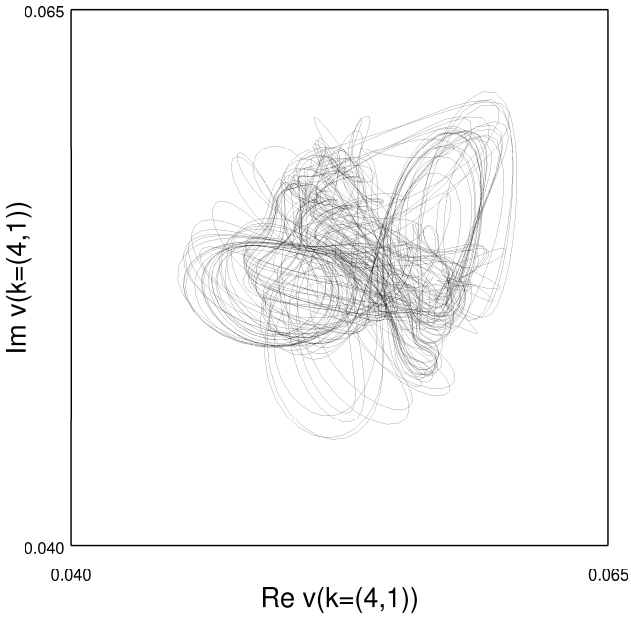

Figure 13: Projection of the chaotic solution for $f = 0.14$ onto the plane spanned by the real and imaginary parts of the forced ($\mathbf{k} = (4, 1)$) mode.

satisfying

$$\sum_{i=1}^{j} \lambda_i \geq 0, \tag{19}$$

then

$$D_{\mathrm{KY}} = j - \frac{1}{\lambda_{j+1}} \sum_{i=1}^{j} \lambda_i. \tag{20}$$

We have found $D_{\mathrm{KY}} = 4.33$.

5 DISCUSSION

We have studied the incompressible 2D Navier-Stokes equations truncated on a torus and described in detail a way into chaos for this system. The periodic boundary conditions necessitate some kind of external forcing to enable non-trivial asymptotic states. In accordance with previous work in the field, we have used a forcing in a single Fourier mode. The strength of this forcing has been our bifurcation parameter. We must leave open the question how far our results depend on the special choice of the forcing.

For increasing strength of the forcing the system exhibits a rather complex sequence of bifurcations of steady states, travelling waves, periodic solutions and solutions on two-dimensional tori, leading to chaos. The appearance of a chaotic attractor was verified by calculating the Lyapunov exponents, of which (just) one becomes positive. Our results seem to confirm the Ruelle-Takens scenario for the transition to turbulence.

Finally, it must be mentioned that we cannot be entirely sure that there is a direct transition from the solution on the two-dimensional torus to the chaotic one, and not perhaps a solution on a three-dimensional torus between both. This question can be clarified only by future calculations with a refined step size for the variation of the bifurcation parameter.

Acknowledgement—We are indebted to an anonymous referee for drawing our attention to the fact that the first torus solution is actually a modulated travelling wave. We also would like to thank Ulrike Feudel for her help in the implementation of the steady state continuation program.

APPENDIX

For testing the stability of stationary states of our fluid system, as well as for tracing the corresponding stationary-solution, or equilibrium, branches in the bifurcation diagram, the Jacobian matrix of the system of equations (16)–(17) is needed, for whose elements one finds

$$\frac{\partial(\mathrm{d}v_{\mathbf{k}}^{\mathrm{Re}}/\mathrm{d}t)}{\partial v_{\mathbf{j}}^{\mathrm{Re}}} = -R^{-1}\mathbf{k}^2\delta_{\mathbf{j}}^{\mathbf{k}} + \mathrm{sgn}(\mathbf{k}-\mathbf{j})A_{\mathbf{k}}v_{\langle\mathbf{k}-\mathbf{j}\rangle}^{\mathrm{Im}} + B_{\mathbf{k}}v_{\mathbf{k}+\mathbf{j}}^{\mathrm{Im}}, \tag{A.1}$$

$$\frac{\partial(\mathrm{d}v_{\mathbf{k}}^{\mathrm{Re}}/\mathrm{d}t)}{\partial v_{\mathbf{j}}^{\mathrm{Im}}} = A_{\mathbf{k}} v_{\langle \mathbf{k}-\mathbf{j} \rangle}^{\mathrm{Re}} - B_{\mathbf{k}} v_{\mathbf{k}+\mathbf{j}}^{\mathrm{Re}}, \tag{A.2}$$

$$\frac{\partial(\mathrm{d}v_{\mathbf{k}}^{\mathrm{Im}}/\mathrm{d}t)}{\partial v_{\mathbf{j}}^{\mathrm{Re}}} = -A_{\mathbf{k}} v_{\langle \mathbf{k}-\mathbf{j} \rangle}^{\mathrm{Re}} - B_{\mathbf{k}} v_{\mathbf{k}+\mathbf{j}}^{\mathrm{Re}}, \tag{A.3}$$

$$\frac{\partial(\mathrm{d}v_{\mathbf{k}}^{\mathrm{Im}}/\mathrm{d}t)}{\partial v_{\mathbf{j}}^{\mathrm{Im}}} = -R^{-1}\mathbf{k}^2 \delta_{\mathbf{j}}^{\mathbf{k}} + \mathrm{sgn}(\mathbf{k}-\mathbf{j}) A_{\mathbf{k}} v_{\langle \mathbf{k}-\mathbf{j} \rangle}^{\mathrm{Im}} - B_{\mathbf{k}} v_{\mathbf{k}+\mathbf{j}}^{\mathrm{Im}}, \tag{A.4}$$

where the abbreviations

$$A_{\mathbf{k}} = (\mathbf{e}_{\mathbf{j}} \cdot \mathbf{k})(\mathbf{e}_{\langle \mathbf{k}-\mathbf{j} \rangle} \cdot \mathbf{e}_{\mathbf{k}}) + (\mathbf{e}_{\langle \mathbf{k}-\mathbf{j} \rangle} \cdot \mathbf{k})(\mathbf{e}_{\mathbf{j}} \cdot \mathbf{e}_{\mathbf{k}}), \tag{A.5}$$

$$B_{\mathbf{k}} = (\mathbf{e}_{\mathbf{j}} \cdot \mathbf{k})(\mathbf{e}_{\mathbf{k}+\mathbf{j}} \cdot \mathbf{e}_{\mathbf{k}}) + (\mathbf{e}_{\mathbf{k}+\mathbf{j}} \cdot \mathbf{k})(\mathbf{e}_{\mathbf{j}} \cdot \mathbf{e}_{\mathbf{k}}) \tag{A.6}$$

have been used.

References

[1] E. N. Lorenz. Deterministic non-periodic flow. *J. Atmos. Sci.*, **20**, 130–141, 1963.

[2] C. Boldrighini and V. Franceschini. A five-dimensional truncation of the plane incompressible Navier-Stokes equations. *Commun. Math. Phys.*, **64**, 159–170, 1979.

[3] V. Franceschini and C. Tebaldi. Sequences of infinite bifurcations and turbulence in a five-mode truncation of the Navier-Stokes equations. *J. Stat. Phys.*, **21**, 707–726, 1979.

[4] V. Franceschini, C. Giberti, and M. Nicolini. Common periodic behaviour in larger and larger truncations of the Navier-Stokes equations. *J. Stat. Phys.*, **50**, 879–896, 1988.

[5] V. Franceschini and C. Giberti. Qualitative and quantitative stabilized behavior of truncated two-dimensional Navier-Stokes equations. *Theor. Comput. Fluid Dyn.*, **2**, 185–192, 1991.

[6] V. Franceschini and R. Zanasi. Three-dimensional Navier-Stokes equations truncated on a torus. *Nonlinearity*, **4**, 189–209, 1992.

[7] M. S. Jolly. Bifurcation computations on an approximate inertial manifold for the 2D Navier-Stokes equations. *Physica D*, **63**, 8–20, 1993.

[8] J. Lee. Topology of trajectories of the 2D Navier-Stokes equations. *Chaos*, **2**, 537–563, 1992.

[9] J. Lee. Steady-state simulation of 2D homogeneous turbulence. *Physica D*, **37**, 417–422, 1989.

[10] I. G. Kevrekidis, B. Nicolaenko, and J. C. Scovel. Back in the saddle again: A computer assisted study of the Kuramoto-Sivashinsky equation. *SIAM J. Appl. Math.*, **50**, 760–790, 1990.

[11] J. L. Kaplan and J. A. Yorke. Chaotic behavior of multi-dimensional difference equations. In H. O. Peitgen and H. O. Walther, editors, *Functional Differential Equations and Approximations of Fixed Points*, pages 228–237. Springer-Verlag, Berlin, 1979.